Article

Flexible Pressure and Temperature Microsensors for Textile-Integrated Wearables

Dimitri Emmanuel dos Santos [1,2], **José Bento Queiroz** [1], **Inês Sofia Garcia** [1], **João Vieira** [1], **José Fernandes** [1],
Edoardo Sotgiu [1], **Graça Minas** [2,3], **Maria Bouçanova** [4], **Luisa Mendes Arruda** [5,6], **Raul Fangueiro** [5,6],
Anabela Salgueiro-Oliveira [6,7], **Alar Ainla** [1], **Filipe Serra Alves** [1] **and Rosana Alves Dias** [1,*]

1 INL—International Iberian Nanotechnology Laboratory, 4715-330 Braga, Portugal;
dimitri.santos@inl.int (D.E.d.S.); jose.queiroz@synopsys.com (J.B.Q.); ines.garcia@inl.int (I.S.G.);
joao.vieira@inl.int (J.V.); jose.fernandes@inl.int (J.F.); edoardo.sotgiu@inl.int (E.S.)
2 Center for MicroElectromechanical Systems (CMEMS), UMinho, 4800-058 Guimarães, Portugal;
gminas@dei.uminho.pt
3 LABBELS—Associate Laboratory in Biotechnology and Bioengineering and Microelectromechanical Systems,
4800-122 Braga, Portugal
4 Impetus S.A., 4740-696 Barqueiros, Portugal; mboucanova@impetus.pt
5 Fibrenamics, University of Minho, 4800-058 Guimarães, Portugal; luisa.arruda@fibrenamics.com (L.M.A.);
rfangueiro@det.uminho.pt (R.F.)
6 Centre for Textile Science and Technology (2C2T), University of Minho, 4800-058 Guimarães, Portugal;
anabela@esenfc.pt
7 Health Sciences Research Unit: Nursing, Nursing School of Coimbra (ESEnfC), 3004-011 Coimbra, Portugal
* Correspondence: rosana.dias@inl.int

Abstract: Environmental factors, such as pressure and temperature, are known to contribute to the formation of ulcers that seriously affect bedridden individuals. Researchers have proposed several technologies to achieve the long-term monitoring of those parameters, usually relying on sensing mats, which poses difficulties in correlating the measurements with specific parts of the body. In this work, we aim to develop microsensors to be integrated into patient clothing. They should be highly flexible, thin with a small footprint, and can be achieved by taking advantage of the microfabrication on polyimide (PI) thin-film substrates (total device thicknesses below 30 μm). Both resistive and capacitance transduction mechanisms were explored, targeting operation ranges of 1 to 40 kPa and 24 to 42 °C. The sensors were integrated into textiles using silicone elastomers and electrical connections based on conductive silver yarn. The experimental characterization showed a nominal capacitance of 21 pF, a sensitivity of -8.44 fF/kPa for the pressure sensors, and a 0.0021 $\Omega/\Omega°C$ sensitivity of the temperature sensor (with resistance of 29 kΩ at 22 °C). The proposed approach can potentially be implemented not only in wearable devices but also in many other applications for health monitoring or human–machine interfaces.

Keywords: flexible sensors; textile integration; pressure microsensors; temperature microsensors

1. Introduction

Pressure ulcers represent a significant health problem affecting bedridden individuals with reduced mobility, resulting in a high socioeconomic burden worldwide [1,2]. There are environmental factors known to contribute to the development of ulcers, most notably pressure, shear stress, moisture, and temperature [3]. Clinical studies that have evaluated the effects of pressure and temperature parameters on the prevalence of pressure ulcers typically use pressure-sensing mats and temperature-sensing units within the bedding [3], allowing one to map the pressure and temperature distributions over the sensing area. Due to the different body shapes or positioning on the bed, the correspondence of a sensing site to a given point/region of the patient's body may vary, as that relation can only be effectively obtained if the exact positioning of the patient in respect to the sensing mat is

known. For long-term pressure/temperature-monitoring systems, the interpretation of the data requires information on the patient's position in the bed or posture detection and recognition algorithms [4,5]. The integration of sensors into the clothing would have the advantage of enabling direct correlation of each sensor measurement with a location on the patient's body, independently of their position, since the clothing follows the movements of the patient. The requirements for this particular application are, however, significantly more demanding than for others, especially for what concerns the size–area covered by each sensor and its thickness, mechanical requirement for flexibility, breathability, among others. Therefore, different from some other applications, having ICs or batteries at the sensor location is not an option (unless these were sub mm thick with an area below 1 cm^2).

Several sensor–textile integration approaches have been explored and described in the literature with different sensor integration levels ranging from high integration level using functional fibers (such as conductive, piezoelectric, or piezoresistive [6–8]) within the textile (woven/knitted) products to lower integration-level alternatives using encapsulated integrated circuits with sensors and electronics soldered on flexible PCBs (printed circuit boards) and flexPCB-based connections [9] and intermediate approaches in between. Polyimide-based (PI, also known as Kapton$^®$) sensors, in particular, have been employed by directly using flexible strips (containing sensing regions) as threads, with or without textile coverings [10–16]. Polyimide is a polymer compatible with the microfabrication of thin-film sensors [17], such as tactile, pressure [18], and moisture sensors, either with capacitive [19] or resistive [20] transduction. The degree of biocompatibility and skin compliance [21] is also an advantage.

The performance of microfabricated sensors is highly reliable and can be tuned to reach suitable specifications for the required application. The high levels of maturity and standardization of the microfabrication technologies (derived from the semiconductor industry) are one of the main advantages in respect to sensor concepts focusing on material developments [22–24]. The highly uniform processes of microfabrication allow for the implementation of thousands of sensors on a single silicon wafer, with reliable and reproducible results and performance. Some flexible substrates are compatible with microfabrication on silicon substrates, with PI being a well-established one. Once released from the rigid support wafer, flexible microsensors are made possible. Flexible and miniature microsensors can offer the monitoring of temperature and pressure in a single device without compromising the comfort and breathability of the clothing. Although PI is not breathable, the flexible strip can be microfabricated perforated or just small enough to not compromise the breathability of the overall textile product. The integration of multiple active sensors on textile products always relies on conductive threads to connect the sensing array/matrix; otherwise, each sensing unit would require its own (bulkier) power and data transmission electronics.

In this work, the development and integration of sensors in textile, for clothing-based long-term monitoring of pressure and temperature, are presented, requiring flexibility, washability, and small form factor. The explored approach takes advantage of polyimide substrates to microfabricate the pressure and the temperature sensors, and the integration approach takes advantage of elastomers, flexible printed circuits boards (flex PCBs), and conductive yarns (in the targeted application the sensors are meant to be connected to an electronic readout module located out of the critical sensing regions). Microfabricated PI pressure sensors have not been previously been integrated into textile, with the use of piezoresistive materials being the main approach pursued in pressure/force-sensing wearables, usually with low detection limits [3,25,26]. The advantage of microfabricated sensors is the high level of control over geometrical features (the microfabrication processes used are well established) and, therefore, performance, namely sensitivity. The advantage of the proposed integration approach in regard to approaches with locally integrated sensor readouts (such as in [9]) is that, locally (at the sensing site, which is prone to pressure injuries), the impact of the solution on the degree of flexibility, thickness, and breathability of the textile product is kept to a minimum. This solution can also easily be

adopted by industry using conductive fiber placement and embroidery techniques coupled with screen printing (for the elastomers), which is an advantage over more integrated approaches described in the literature (such as in [10–16]). As these sensors are meant to integrate garments, the electronic connections of these sensors are accomplished using a commercially available conductive yarn, which can conduct the sensor signals to a remote garment location where an electronic readout module can be accommodated (as opposed to the pressure-injury-prone sites). Inductive coupling could also have been considered but presents the disadvantage of requiring large areas with conductive yarn (which is undesirable given its lack of stretchability).

2. Design and Fabrication

Since pressure and temperature sensors have different requirements, herein, they are discussed separately, although layouts have been prepared with both sensors integrated in the same device. From clinical studies, it can be concluded that the ranges targeted should include at least 1–40 kPa [27–30]. As for the temperature, a conservative range (concerning the human skin temperature range [31]) of 20–45 °C was selected. The optimization criteria for the design took into account the maximization of sensitivity within these target operation ranges, e.g., small size (footprint and thickness) and microfabrication constraints (such as minimum feature size and spacing of 10 microns).

2.1. Sensors Design and Modeling

Regarding the pressure sensors, both capacitive and resistive approaches were pursued in parallel. Capacitive approaches are commonly used since they provide low power consumption and can be fabricated in a more standard process. Resistive transduction is, however, more compatible with large matrices of sensors (in terms of electronic readout requirements) but usually requires additional piezoresistive materials upon fabrication. Contact-mode resistive sensor implementations are less standard [32,33] and have not been demonstrated in polyimide thin-film substrates. Resistive mode, though, has a great advantage for the implementation of large matrices, as it does not require large integration times, usually associated with the electronic readout of small capacitive sensors.

2.1.1. Pressure Sensors

For pressure sensing, both transduction mechanisms considered (resistive—RPS and capacitive—CPS) relied on pressure-deformable thin-film membranes with an air gap in between (patterned using a sacrificial layer of SiO_2, as explained further in the microfabrication process section). The resistive approach is based on the varying contact area between two metal electrodes, one of them double spiral-shaped (Figure 1). The top electrode consisted of a continuous metal plate of aluminum (in particular, AlSiCu (94% Al, 5% Si and 1% Cu), a standard in the semiconductor industry), while the bottom electrode took the shape of a double Archimedean spiral made of platinum (Pt), with a defined nominal resistance. As isotropic pressure is applied (while the sensor is held against a hard surface), the top (continuous metal) membrane deforms and shortens the double spiral current path, from the center to its borders, decreasing the measured resistance at the double-spiral ends/contacts.

As for the capacitive approach, it was based on the micromembrane parallel-plate capacitor design, in touch-mode operation [18]. In other words, the model used accounts for the capacitance increase while the plates approached (but not touching), and the capacitance increase that continued after contact between the membranes was established (due to further deformation and contact area increase). In this design, both the top and bottom capacitor plates are continuous and enclosed by a polyimide dielectric with an air gap in between (Figure 2).
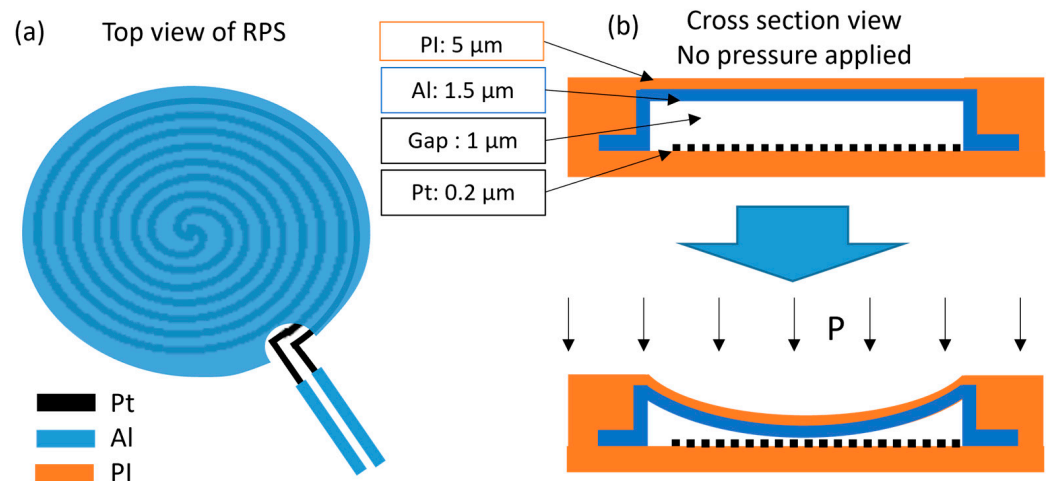
Figure 1. Schematic of top view (**a**) and cross-section view (**b**) (with and without applied pressure) of the resistive pressure sensor concept.
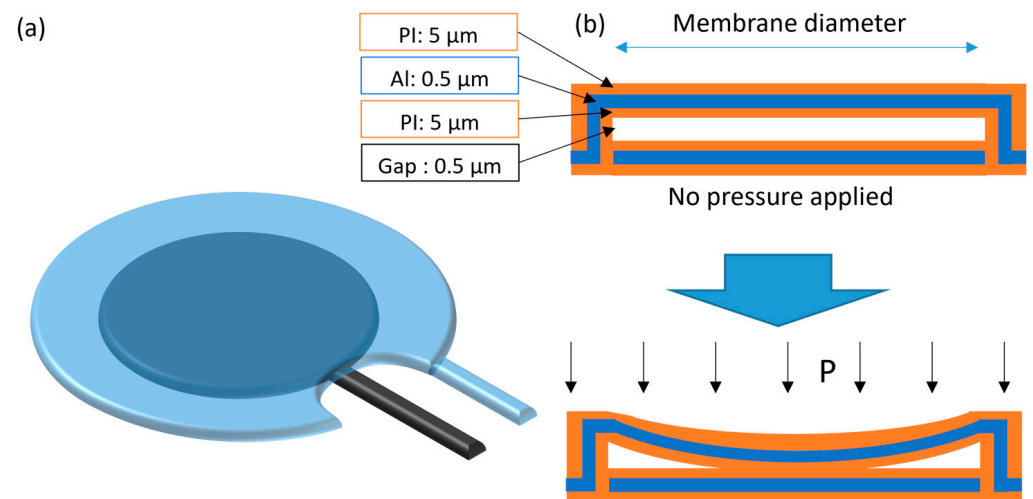

Figure 2. Illustration of the capacitive pressure sensor (**a**) and its cross-section (**b**) with and without pressure applied.

Analytical models of the flexible structures with membrane electrodes and air cavities were implemented in order to select the most suitable range of diameters for the membranes. Based on the geometry parameters and material properties, the models calculate the mechanical deformations and the electrical capacitance (for the CPS) or electrical resistance (for the RPS) variation in the structures. Figure 3 shows the simulated capacitance and resistance variations with different applied pressures for membrane diameters of 0.75, 1, and 1.5 mm, which correspond to nominal capacitances (C0) of 1.1 pF, 2.2 pF, and 4.4 pF, and nominal resistances of 8.5 kΩ, 3.9 kΩ, and 1.8 kΩ, respectively. In short, larger membrane diameters deflect more, therefore, showing larger normalized capacitance variations, as well as allowing one to accommodate larger double-spiral-shaped electrodes underneath it, which translates to larger resistance variations. However, CPSs with a membrane diameter of 0.75 mm were selected for fabrication, due to higher linearity in the target pressure range while showing a 10% relative change in capacitance at 40 kPa. Regarding RPS, membranes with diameters of 0.75 mm, 1.0 mm, and 1.5 mm were fabricated.
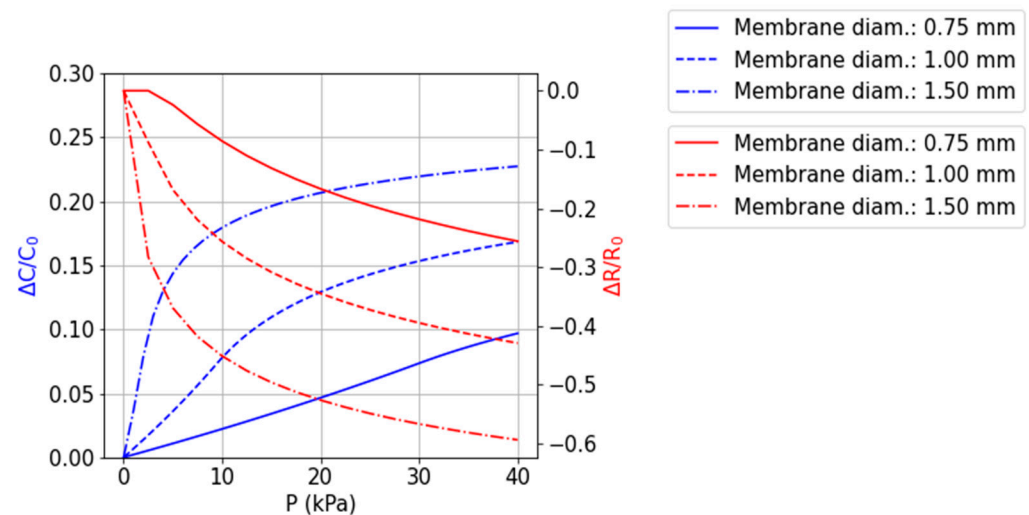
Figure 3. Simulated performance of capacitive and resistive variations in the range 0–40 kPa, for 3 different membrane diameters (single membrane response). Membrane diameters of 0.75, 1, and 1.5 mm, correspond to nominal capacitances of 1.1 pF, 2.2 pF, and 4.4 pF, or nominal resistances of 8.5 kΩ, 3.9 kΩ, and 1.8 kΩ, respectively.

2.1.2. Resistance Temperature Detectors (RTDs)

For the temperature sensors and taking advantage of the compatibility with the RPS fabrication process, the well-established resistive temperature detector (RTD) technology was used, by designing current paths in a circular shape around the RPS, as seen in Figure 4 (black wire). Platinum (Pt) was used given its high linearity in an extended temperature range, as well as its high electrical resistivity (in comparison to other available metals (Figure 4) and chemical inertness [34].
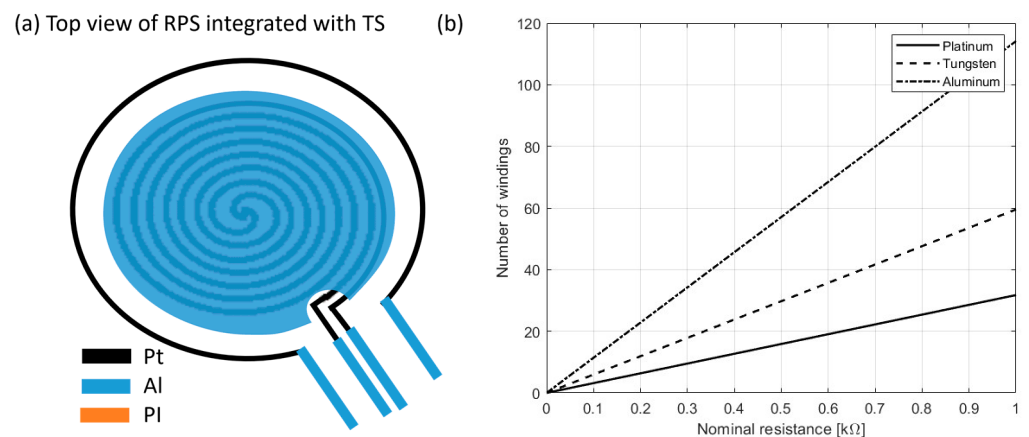

Figure 4. Schematic of the RPS top view including an RTD (**a**) and relation between nominal resistance and number of windings around a pressure sensor (**b**).

2.2. Sensor Microfabrication and Textile Integration

Two microfabrication runs were executed: one for the RPS and temperature sensors and one for CPS. The fabrication of the CPS is simpler and has fewer materials and process steps involved. Therefore, although the microfabrication of both the CPS and RPS is compatible to be integrated, these were fabricated in different microfabrication runs.

Each PI layer was 5 μm thick, and the SiO_2 sacrificial layer (to define air gap) was 1 μm on the RPS and 500 nm on the CPS. The aluminum and platinum layers (AlSiCu and Pt) were 1.5 μm and 200 nm thick, respectively.

2.2.1. Microfabrication Process Flow

Figure 5 illustrates the process flow of the RPSs combined with the platinum RTDs. The SiO$_2$ was deposited by PE-CVD (plasma-enhanced chemical vapor deposition), polyimide by spin coating, and metals by sputtering. The SiO$_2$ sacrificial layers, the PI, and the AlSiCu/TiW metals were patterned via lithography followed by reactive ion etching (RIE), while the platinum was patterned by lift-off.
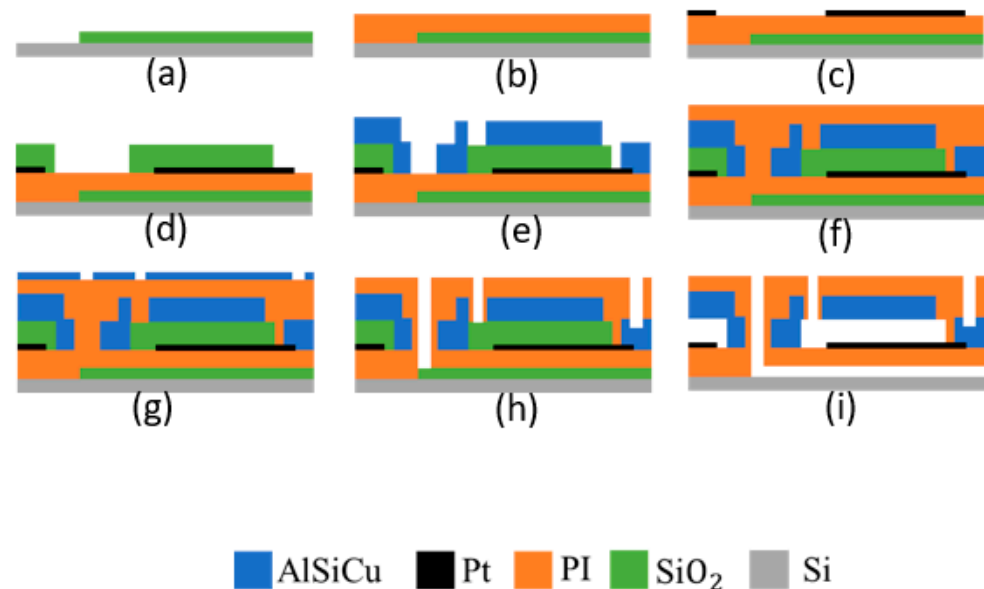

Figure 5. Microfabrication process flow: (**a**) SiO$_2$ deposition on silicon substrate and patterning, (**b**) PI spin coating, (**c**) Pt sputtering and patterning by lift-off, (**d**) SiO$_2$ deposition (PE-CVD) and patterning by RIE, (**e**) top electrode metal (Al and TiW multilayer) deposition and patterning by lithography and RIE, (**f**) PI spin coating at 3900 rpm for 30 s, (**g**) metal hard mask (Al and TiW bilayer) deposition and patterning, (**h**) PI RIE and hard mask wet etch, (**i**) HF (hydrofluoric acid) vapor release.

The CPSs were fabricated in a microfabrication run similar to the one described in [18], for simplification purposes. The process flow of the CPS consists of:

(a) SiO$_2$ deposition (by PE-CVD) on silicon substrate;
(b) Spin coating of 1st layer of 5 μm of PI;
(c) Bottom electrode metal sputtering and patterning by lithography followed by RIE;
(d) Spin coating of 2nd layer of 5 μm of PI;
(e) SiO$_2$ deposition and patterning by lithography and RIE;
(f) Spin coating of 3rd layer of 5 μm of PI;
(g) Top electrode metal (AlSiCu and TiW multilayer) deposition and patterning by lithography and RIE;
(h) Spin coating of 4th (and last) of 5 μm of PI;
(i) Metal hard mask (AlSiCu and TiW bilayer, 600 nm total thickness) deposition and patterning;
(j) PI RIE and hard mask wet etch;
(k) HF vapor release.

The electrode metals consisted of a multilayer stack with a total of 1000 nm of AlSiCu and 200 nm of TiW.

2.2.2. Layouts and Fabricated Sensors

The fabricated layouts (Figure 6) included RPSs with 3 × 3 membrane arrays per device, with the double-spiral-shaped coils connected in series, and CPSs with four membranes with the capacitive electrodes connected in parallel. This increases the nominal resistance/capacitance values at the same time that it allows for the determination of the

average pressure over the area of the array and minimizing the influence of membrane differences due to microfabrication process non-uniformities. The RTDs were patterned around the RPS layouts.
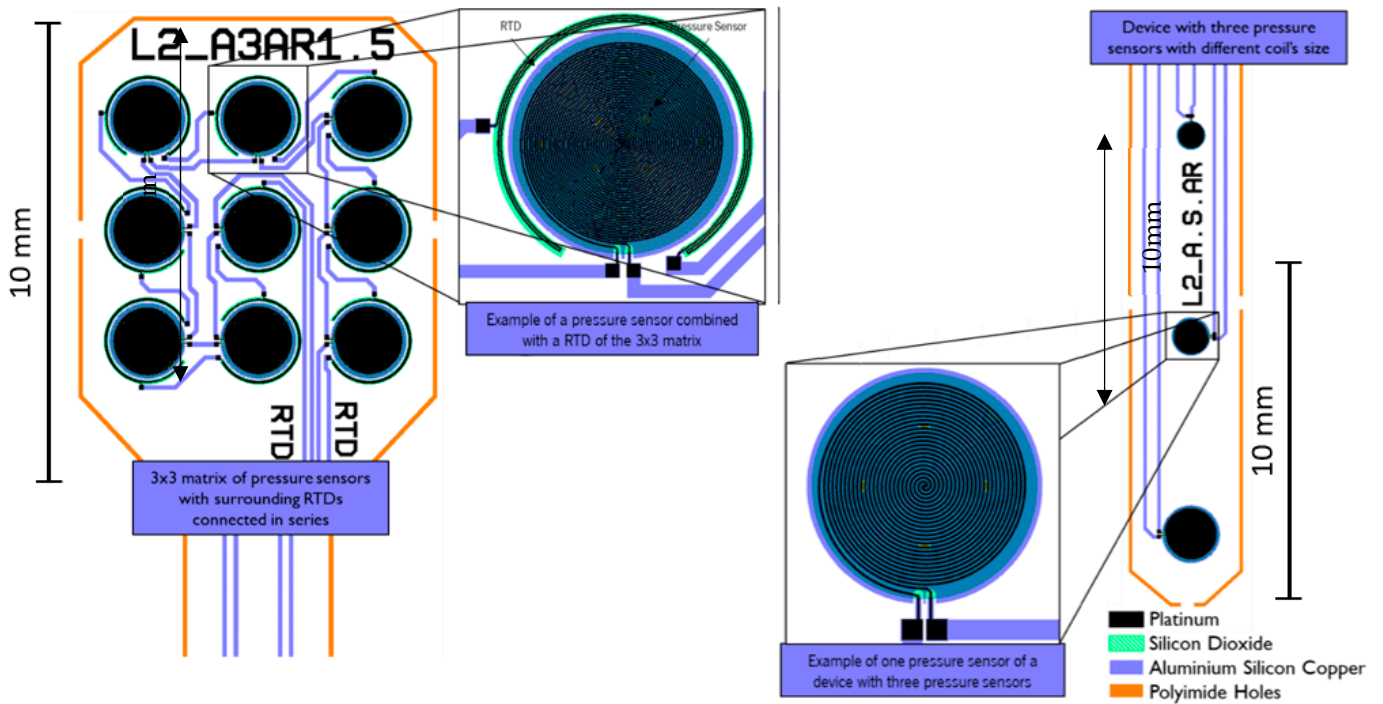

Figure 6. Layouts of the RPS with RTDs and the CPS.

The fabricated devices (Figure 7) include both electrical pads compatible with FPC-FFC (Flexible Printed Circuit–Flat Flexible Cables) connectors for the device characterization and 2 mm by 4 mm pads for direct embroidery tests.
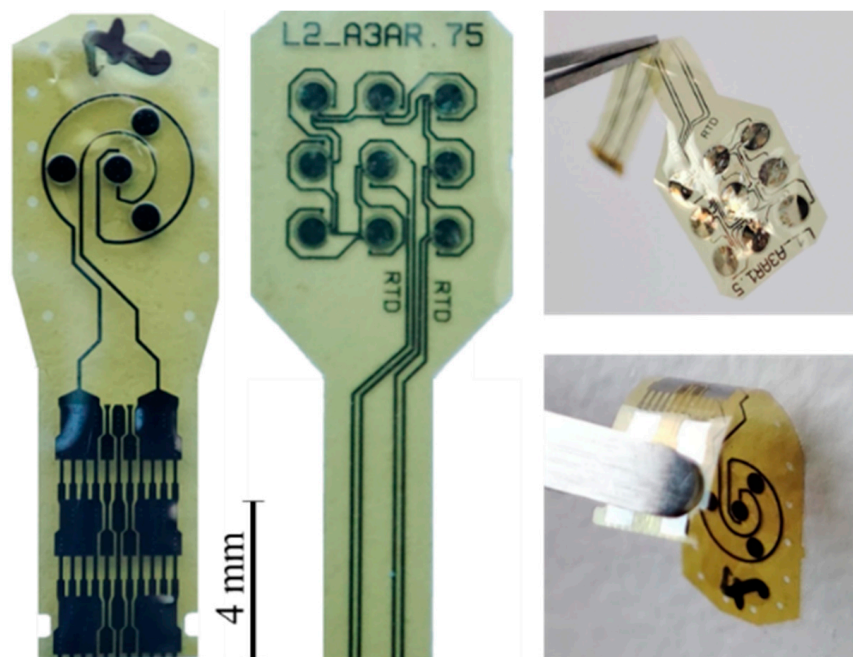

Figure 7. Pictures of the fabricated sensors.

The microfabrication process of the RPS devices presented more challenges than their CPS counterparts. Delamination and electric shorts problems occurred, which are currently being addressed in order to reach a suitable yield with functional devices.

2.2.3. Textile Integration

In order to preliminarily assess the sensor performance after textile integration, the sensors must be assembled on a textile substrate. For this, two approaches have been tested. One consisted of direct connection of the PI sensors with conductive textile yarns through embroidery on its electrical pads, and the other on connecting the sensors to an intermediate custom-designed flexible PCB, through transversely conductive tape (aka z-tape), which is then itself connected with the conductive yarn through embroidery. Since the flexPCB pads have thicker metal and dielectric support layers, this solution is expected to be mechanically (and electrically) more robust than direct embroidery connection. Using direct embroidery is more compatible with a thin and highly flexible solution and, consequently, more appropriate for clothing where the weight of the body is constantly exerting pressure on the skin against the fabric.

The embroidery was made using a sewing machine, straight stitch, with a commercially available extrinsically conductive silver yarn (polyethylene terephthalate yarn, silver coated by plasma technology, with 78 Dtex and a conductivity of 1.3 Ω/cm from Swicofil, Switzerland [35]), guaranteeing the piercing of the electrode pads by the conductive thread. Figure 8 shows pictures of both approaches. This yarn is not stretchable, so in order to maintain stretchability in the final application, it must be warranted though the embroidery design instead (using for instance a zigzag configuration). It is highly conductive and can sustain wear and tens of household washing cycles without significant material deterioration [35].
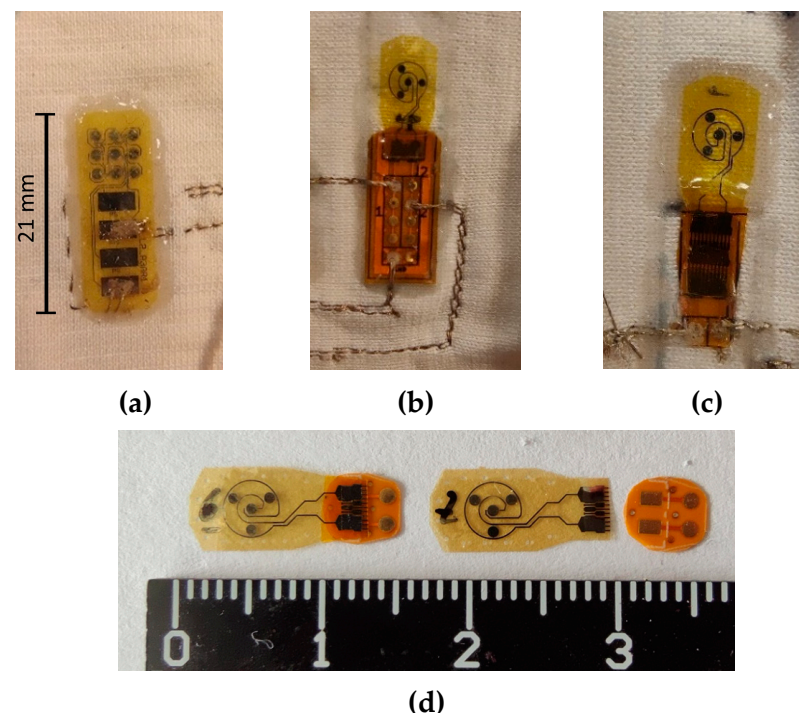

(a)   (b)   (c)

(d)

Figure 8. Textile integration of (**a**) an RPS by direct embroidery, (**b**) a CPS by using an intermediate flexPCB, and (**c**) a CPS with a smaller flexPCB version. Both flexPCB and sensor can be further miniaturized (**d**).

It was readily observed that the intermediate PCB (100 μm thick) improved the mechanical and electrical connection robustness of the integrated sensors (otherwise, the connection would be intermittent upon pressing or bending the sample). To additionally

improve the electrical connections, a conductive epoxy (with ~24.6% w/w Ag powder) was prepared and applied to the pierced electrodes (both on the PI sensors and the flexPCB pierced pads).

Different formulations of silicone elastomers were tested for direct attachment of the polyimide sensors to the fabric and for improving mechanical integrity (with varying working viscosities before curing and resulting Young's modulus after curing). Ecoflex$^{®}$ was selected for its easy preparation and application and for the resulting mechanical characteristics, such as elasticity (although other materials could have been used with different results in terms of elasticity and adhesion to the textile and the sensor) [36]. Polyimide is a moisture-absorbing material [17], so embedding it in elastomer also confers protection by stabilizing the material properties.

The main disadvantages of using a conductive yarn are their lack of stretchability and possible roughness to touch. As mentioned, the stretchability of the conductive path can be improved by embroidery path design (at the expense of additional resistance, since this is not the shortest path). The roughness may be mitigated by local coverage with textile industrial coatings. The reasoning for using conductive yarn to connect the thin-film sensors to a remote readout and transmission module versus using electronic components at each sensor site is highly dependent on the final application requirements. For pressure-injury-prone sites, the former was considered more appropriate. In real-world use, any fluid leak or spillage would short-circuit the exposed contacts, but that information is also useful since that situation warrants the replacement of the garment given that moisture is also a risk for pressure injuries.

2.3. Experimental Setup for Sensor Characterization

For the characterization of the pressure sensors, a Shimadzu Autograph AGX-V precision universal tester tool, coupled with a 50 N load cell, was used to apply pressure to the device (Figure 9). An Agilent multimeter was used for the RPS readout, while for the CPS, a C2D (capacitance to digital)-based readout (PCAP02 Evaluation module, ScioSense B.V., Eindhoven, The Netherlands) was employed. An Ecoflex™ disk of 1 cm diameter and 1 mm thickness was used as an interface between the load cell probe (flat metal surface) and the sample in both RPS and CPS.
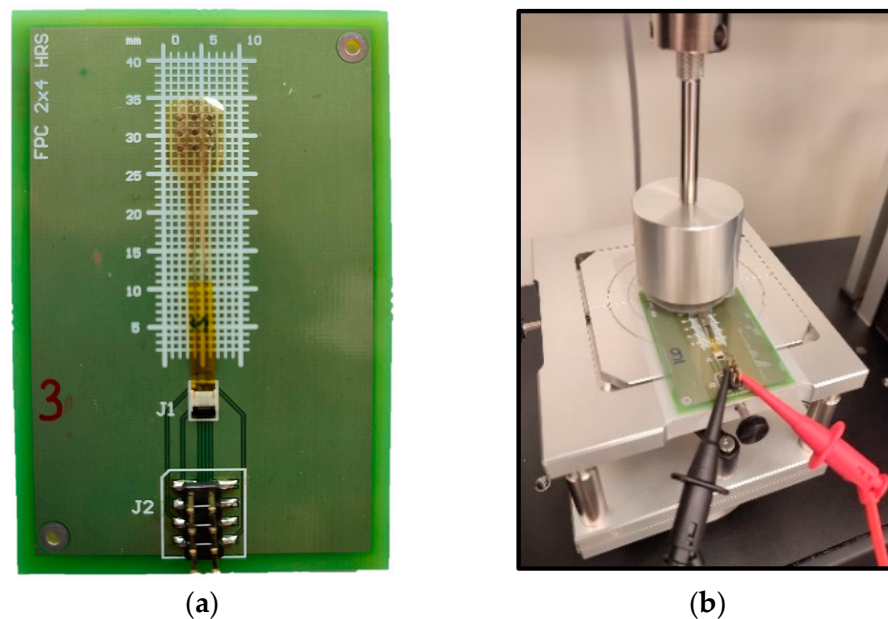

(**a**) (**b**)

Figure 9. 2 cm long device connected to FPC-FFC connector on PCB (**a**) and mounted on the pressure characterization setup (**b**).

The RTDs were characterized using a Weiss WKL 34 climate chamber (allowing us to perform temperature tests in an enclosed environment with electrical connection to the outside). Matlab® scripting was used to both remotely control the climatic chamber temperature settings and collect the RTD values using an Agilent multimeter (using a 100 µA current).

3. Results and Discussion

The RPS devices suffered from short circuiting between electrodes, compromising the yield and impairing electrical characterization.

The RTDs, fabricated in the same devices as the RPS, were tested in the climatic chamber, before textile integration. At that time, the RTDs showed a quasi-linear behavior, following the expected theory (Figure 10). The prior characterization (by sheet resistance measurement in the climatic chamber) of the unpatterned sputtered platinum films annealed at 300 °C (the maximum temperature the sensors are exposed to) showed a resistivity of 5.24×10^{-7} Ωm (above the 10.5×10^{-8} Ωm bulk value at 20 °C) and a thermal coefficient of 0.0021/°C (below 0.00385/°C of bulk platinum). Using these experimental values, the nominal resistance expected for the RTD (3-by-3 matrix, with three circular windings around a 1 mm diameter per cell, trace width of 10 µm) was 22 kΩ. The deviation in the experimental nominal resistance (close to 29 kΩ) can be explained by microfabrication deviations in feature width and the additional resistance of the connection traces. The measured sensitivity of the temperature sensor was 6.06 mV/°C (for 100 µA) or 0.0021/°C (aligned with the characterized platinum thin films). After textile integration, the electrical connections (by direct embroidery) were compromised, not displaying enough stability in the sample resistance to comply with the characterization setup.
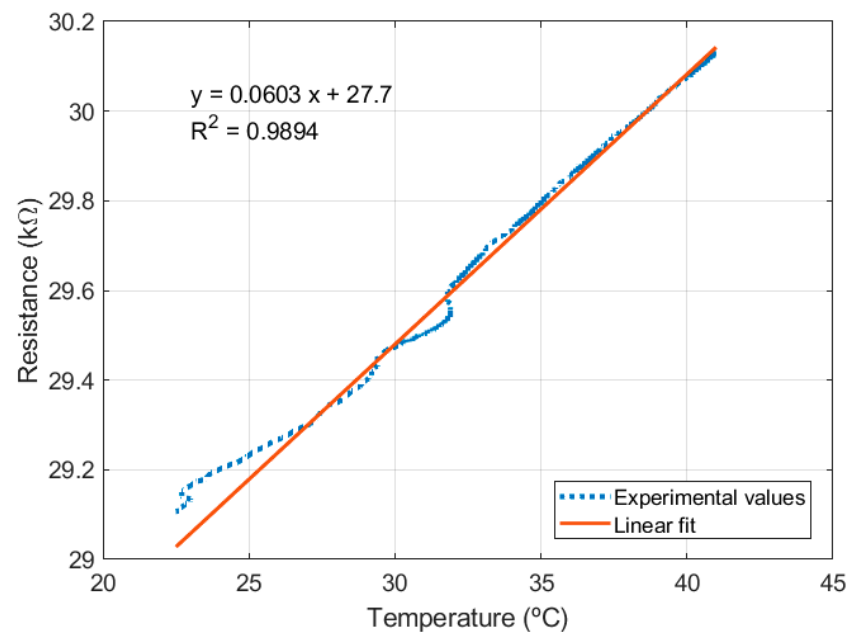

Figure 10. RTD resistance variation.

CPS devices were tested before and after textile integration by applying cyclic pressure between 5 and 40 kPa (10 cycles). The results, depicted in Figures 11 and 12, show that the integration resulted in a nominal capacitance change from 22 pF to 21 pF and a decrease in the total capacitance variation (ΔC = 0.45 pF before and ΔC = 0.40 pF after integration). The capacitance variation profile after integration shows an asymmetry between increasing and decreasing pressure, which can arise from non-uniformities in the Ecoflex™ sensor–textile assembly.
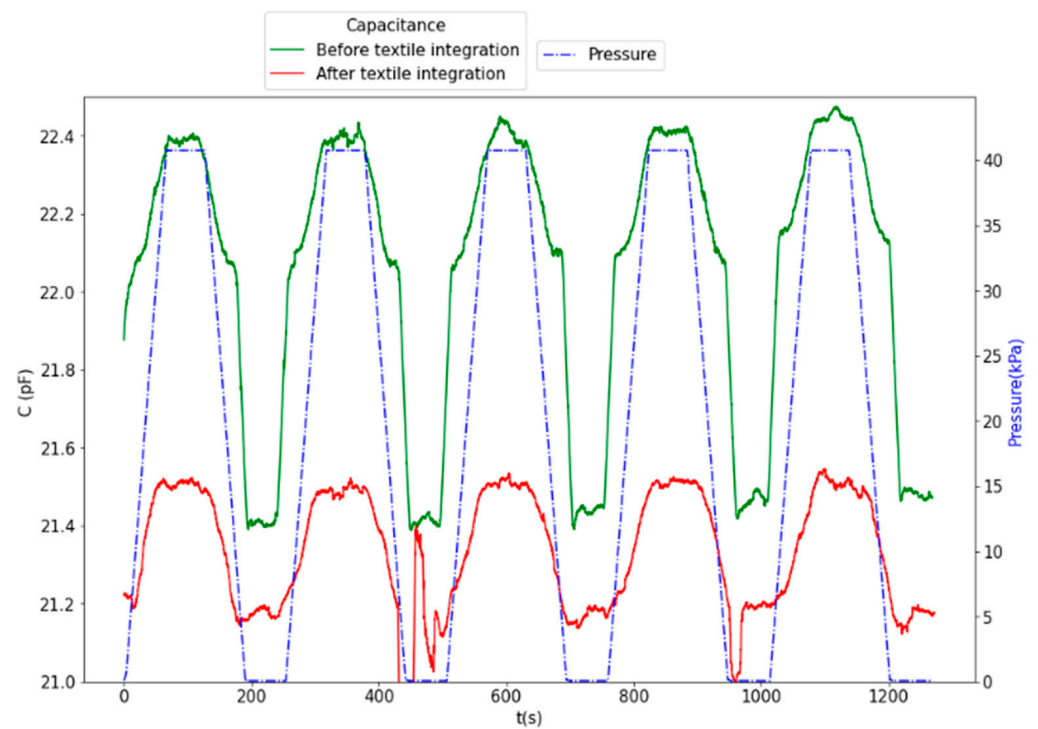
(**a**)
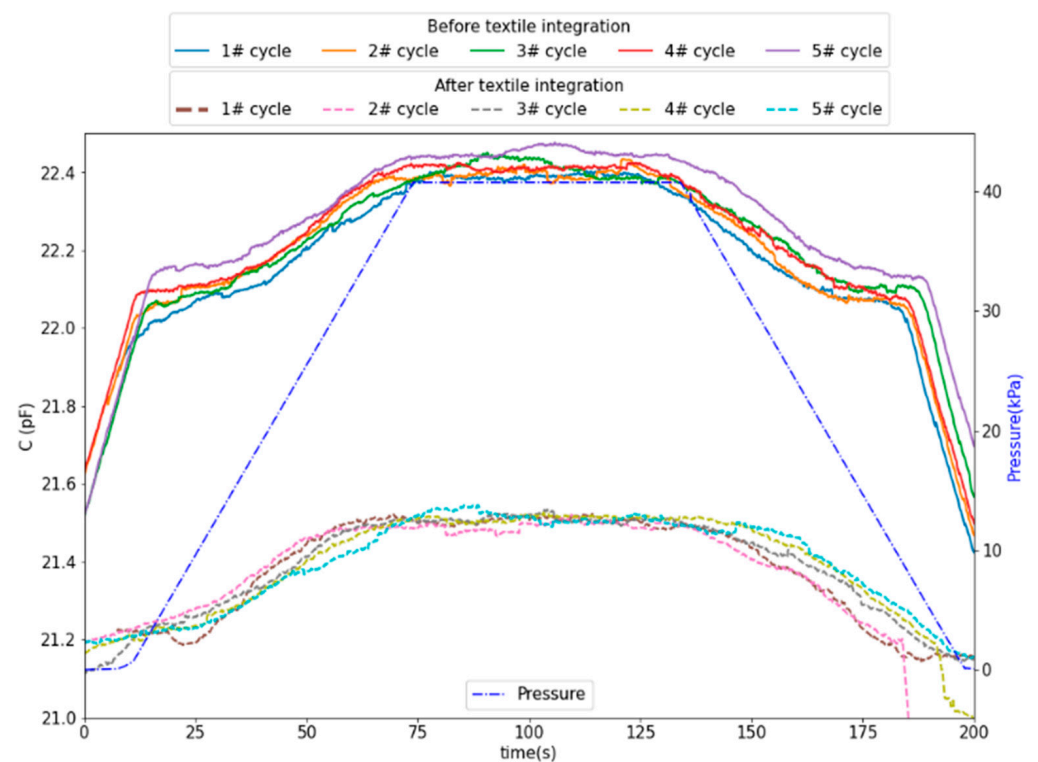
(**b**)

Figure 11. CPS response before textile integration (variation of 0.45 pF over a 22 pF nominal value) and after textile integration (variation of 0.4 pF over a 21 pF nominal value): (**a**) overall time series and (**b**) superposition of all cycles.
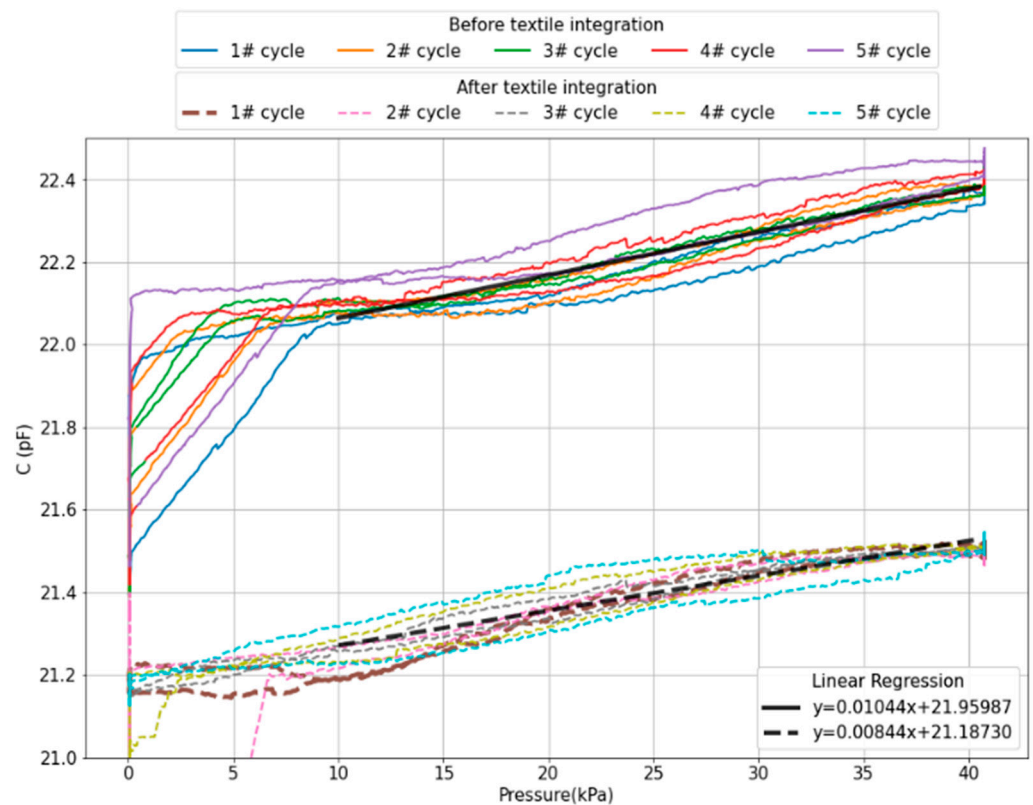
Figure 12. Capacitive response with applied pressure before (solid lines) and after (dashed lines) textile integration.

The response of the CPS showed a drift of 0.075 pF after 1000 s before textile assembly (green line in Figure 11a), which was not noticeable afterwards, which may result from the additional Ecoflex layer that supports a fast and uniform pressure distribution, as opposed to the thinned Ecoflex disc attached to the force displacement probe.

From the linear fitting to the data in Figure 12, the average sensitivity within the linear range of 10 to 40 kPa obtained is 10.4 fF/kPa before integration and 8.44 fF/kPa after integration, which translates to a sensitivity decrease of approximately 19%. Below 10 kPa, stiction was observed between the probe and the sensor, resulting in a pulling effect between the sensor membranes and decreased the capacitance.

While the results were reasonably similar before and after textile integration, we observe a significant discrepancy in respect to expected nominal capacitance and sensitivity. This is attributed to parasitic capacitances that strongly depend on the electronic measurement setup. Despite the magnitude of the measured capacitance (22 pF) being approximately 5-times higher than the capacitance expected for the parallel-plate sensor only (array of four membranes with 1.1 pF each), the used C2D-based readout provides enough resolution to accommodate this external interference. A way to further increase the robustness to parasitic capacitances is to add multiple plates in parallel, therefore increasing the nominal capacitance while maintaining normalized sensitivity.

From a comparison with the literature, in terms of sensing performance, the proposed sensor exhibits values in line with the state of the art (Table 1).

Table 1. Selected characteristics comparisons on the previous study and this work.

Work	Measurement Mechanism/ Change	Pressure/Force Range	Sensitivity	Note
E.Sotgiu et al. [18]	interelectrode spacing	30 kPa, 80 kPa	1, 0.43 fF/kPa (bare)	Flexible PI-based device, bare or PDMS coated
M.Y. Cheng et al. [37]	interelectrode spacing	0.1 N	~1.67%/mN	Measuring normal/shear force, PDMS
H.-K. Lee et al. [38]	interelectrode spacing	250 kPa	1.2–1.3%/mN	Measuring normal/shear force, PDMS
J. Dobrzynska et al. [39]	interelectrode spacing	100 N	0.5–1 fF/N	Finger-like microstructures, PI, no air gap
Y.-C. Wang et al. [40]	interelectrode spacing	10 kPa	1.9 pF/N	A mutual capacitive touch panel, PET/PDMS
G. Liang et al. [41]	interelectrode spacing	0.5 N, 4 N	~67.2, 7.7%/N	Measuring normal/shear force, PDMS
M. Chandra et al. [42]	overlap area	2 N	~0.08 pF/N	Measuring normal/shear force, PET/PDMS
This work	interelectrode spacing	1 to 40 kPa	8.44 fF/kPa	Flexible PI-based device

By focusing on the integration of the sensing units and the electronics on the textile, the fabrication process ranges from the conventional rigid electronics attached to textiles to electronic components made from active conductive yarns. Indeed, the solutions proposed in [43,44] of fabricating mechanically flexible active electronic devices directly in the fabrics are complex and expensive. The solution proposed in this work aims to be an alternative approach in the integration of flexible electronics into fabrics, representing a good compromise between the mechanical and electrical properties of the final device.

The sensors integrated in textile were the subject of a mixed-method study with a focus group from the nursing field [45]. The parameters defined for evaluation were adequacy regarding stiffness, roughness, imprinting, and comfort. The sensors were not evaluated in isolation but coupled with interface flexPCBs (either attached to it though z-axis conductive tape or attached to a different region of the textile and interconnected to the flexPCB through embroidery). The approach using intermediate flexPCB was considered, in general, moderately adequate for bedridden patients, particularly due to the flexPCB's rigidity and embroidery roughness. Different studies associate the development of new technologies to monitor changes in skin (pressure and temperature) to a more effective prevention of pressure ulcers, compared to diagnosis only by observation [46–48], in particular because wearables can trigger interventions and inform care delivery [49].

4. Conclusions

This work focused on the development of microfabricated sensors suitable for textile integration in applications where the bulkiness of the sensing solution is a major constraint. It aimed, therefore, to demonstrate the design and microfabrication of flexible substrate-based pressure and temperature sensors and its integrability into textile products (although the integration process requires further optimization and testing).

Both resistive and capacitive transduction mechanisms were explored, targeting operation ranges of 1 to 40 kPa and 24 to 42 °C, although the resistive pressure-sensing approach needs further validation. The sensors were assembled post-fabrication on textile using silicone elastomers and conductive thread-based electrical connections with reasonably similar response before and after assembly.

Although the footprint of the polyimide pressure and temperature microfabricated sensors can be further minimized, we conclude that these microsensors can be integrated

into patients clothing, resulting in a flexible and thin solution for monitoring pressure to prevent ulcer development.

Further work consists of characterization of the pressure sensor sensitivity with different curvature angles (bending tests) and evaluation of washability and reproducibility, as well as changes in the type of yarn and type of stitch. Future work will also include the assessment of multi-cycle durability.

Author Contributions: Conceptualization, R.A.D., F.S.A. and A.A.; methodology, R.A.D., F.S.A., A.A., D.E.d.S., J.F. and J.B.Q.; software, D.E.d.S., J.B.Q. and J.V.; validation, J.B.Q., J.V. and D.E.d.S.; formal analysis, J.B.Q., R.A.D., F.S.A. and J.V.; investigation, D.E.d.S., J.B.Q., R.A.D., F.S.A., A.S.-O. and I.S.G.; resources, J.F., E.S., L.M.A., M.B., G.M. and R.F.; writing—original draft preparation, D.E.d.S., J.B.Q., R.A.D. and J.V.; writing—review and editing, R.A.D., F.S.A., G.M. and E.S.; visualization, J.V.; supervision, R.A.D. and F.S.A.; project administration, R.A.D.; funding acquisition, R.A.D. All authors have read and agreed to the published version of the manuscript.

Data Availability Statement: Data are contained within the article.

Conflicts of Interest: The authors declare no conflicts of interest.

List of Acronyms

C2D	capacitance to digital
CPS	capacitive pressure sensor
flexPCB	flexible printed circuit board
FPC-FFC	flexible printed circuit–flat flexible cables
HF	hydrofluoric acid
PCB	printed circuit board
PE-CVD	plasma enhanced chemical vapor deposition
PI	polyimide
RIE	reactive ion etching
RPS	resistive pressure sensor
RTD	resistive temperature detector

References

1. Chung, M.; Widdel, M.; Kirchhoff, J.; Sellin, J.; Jelali, M.; Geiser, F.; Mücke, M.; Conrad, R. Risk Factors for Pressure Ulcers in Adult Patients: A Meta-analysis on Sociodemographic Factors and the Braden Scale. *J. Clin. Nurs.* **2022**, *32*, 1979–1992. [CrossRef]
2. da Silva Galetto, S.G.; do Nascimento, E.R.P.; Hermida, P.M.V.; Busanello, J.; de Malfussi, L.B.H.; Lazzari, D.D. Medical device-related pressure injuries in critical patients: Prevalence and associated factors. *Rev. Da Esc. Enferm.* **2021**, *55*, e20200397. [CrossRef] [PubMed]
3. Silva, A.; Metrôlho, J.; Ribeiro, F.; Fidalgo, F.; Santos, O.; Dionisio, R. A Review of Intelligent Sensor-Based Systems for Pressure Ulcer Prevention. *Computers* **2022**, *11*, 6. [CrossRef]
4. Marchione, F.G.; Araújo, L.M.Q.; Araújo, L.V. Approaches that use software to support the prevention of pressure ulcer: A systematic review. *Int. J. Med. Inform.* **2015**, *84*, 725–736. [CrossRef] [PubMed]
5. Jiang, M.; Ma, Y.; Guo, S.; Jin, L.; Lv, L.; Han, L.; An, N. Using Machine Learning Technologies in Pressure Injury Management: Systematic Review. *JMIR Med. Inf.* **2021**, *9*, e25704. [CrossRef] [PubMed]
6. Knitronix. Available online: https://www.knitronix.com/ (accessed on 14 September 2023).
7. Magniez, K.; Krajewski, A.; Neuenhofer, M.; Helmer, R. Effect of drawing on the molecular orientation and polymorphism of melt-spun polyvinylidene fluoride fibers: Toward the development of piezoelectric force sensors. *J. Appl. Polym. Sci.* **2013**, *129*, 2699–2706. [CrossRef]
8. Meng, K.; Xiao, X.; Wei, W.; Chen, G.; Nashalian, A.; Shen, S.; Xiao, X.; Chen, J. Wearable Pressure Sensors for Pulse Wave Monitoring. *Adv. Mater.* **2022**, *34*, 2109357. [CrossRef]

9. Wicaksono, I.; Kodama, E.; Dementyev, A.; Paradiso, J.A. SensorNets: Towards reconfigurable multifunctional fine-grained soft and stretchable electronic skins. In Proceedings of the Extended Abstracts of the 2020 CHI Conference on Human Factors in Computing Systems, Honolulu, HI, USA, 25–30 April 2020; pp. 1–8. [CrossRef]
10. Atamana, C.; Kinkeldei, T.; Vasquez-Quintero, A.; Molina-Lopez, F.; Courbat, J.; Cherenack, K.; Briand, D.; Tröster, G.; De Rooij, N.F. Humidity and temperature sensors on plastic foil for textile integration. *Procedia Eng.* **2011**, *25*, 136–139. [CrossRef]
11. Mattana, G.; Kinkeldei, T.; Leuenberger, D.; Ataman, C.; Ruan, J.J.; Molina-Lopez, F.; Quintero, A.V.; Nisato, G.; Tröster, G.; Briand, D.; et al. Woven temperature and humidity sensors on flexible plastic substrates for e-textile applications. *IEEE Sens. J.* **2013**, *13*, 3901–3909. [CrossRef]
12. Zysset, C.; Kinkeldei, T.W.; Munzenrieder, N.; Cherenack, K.; Tröster, G. Integration method for electronics in woven textiles. *IEEE Trans. Compon. Packag. Manuf. Technol.* **2012**, *2*, 1107–1117. [CrossRef]
13. Cherenack, K.; Van Pieterson, L. Smart textiles: Challenges and opportunities. *J. Appl. Phys.* **2012**, *112*, 091301. [CrossRef]
14. Cherenack, K.; Zysset, C.; Kinkeldei, T.; Münzenrieder, N.; Tröster, G. Woven electronic fibers with sensing and display functions for smart textiles. *Adv. Mater.* **2010**, *22*, 5178–5182. [CrossRef] [PubMed]
15. Costa, J.C.; Spina, F.; Lugoda, P.; Garcia-Garcia, L.; Roggen, D.; Münzenrieder, N. Flexible Sensors—From Materials to Applications. *Technologies* **2019**, *7*, 35. [CrossRef]
16. Lugoda, P.; Costa, J.C.; Oliveira, C.; Garcia-Garcia, L.A.; Wickramasinghe, S.D.; Pouryazdan, A.; Roggen, D.; Dias, T.; Münzenrieder, N. Flexible temperature sensor integration into e-textiles using different industrial yarn fabrication processes. *Sensors* **2019**, *20*, 73. [CrossRef] [PubMed]
17. Pasahan, A. Sensor Applications of Polyimides. In *High Performance Polymers—Polyimides Based—From Chemistry to Applications*; IntechOpen: London, UK, 2012. [CrossRef]
18. Sotgiu, E.; Aguiam, D.E.; Calaza, C.; Rodrigues, J.; Fernandes, J.; Pires, B.; Moreira, E.E.; Alves, F.; Fonseca, H.; Dias, R.; et al. Surface Texture Detection with a New Sub-mm Resolution Flexible Tactile Capacitive Sensor Array for Multimodal Artificial Finger. *J. Microelectromechanical Syst.* **2020**, *29*, 629–636. [CrossRef]
19. Liu, R.; Huang, J.-Q.; Huang, Q.-A. A Capacitive Humidity Sensor Based on an PTFE sSubstrate. *Sensors* **2017**, *17*, 1009. [CrossRef]
20. Dubourg, G.; Segkos, A.; Katona, J.; Radović, M.; Savić, S.; Niarchos, G.; Tsamis, C.; Crnojević-Bengin, V. Fabrication and characterization of flexible and miniaturized humidity sensors using screen-printed TiO2nanoparticles as sensitive layer. *Sensors* **2017**, *17*, 1854. [CrossRef]
21. Constantin, C.P.; Aflori, M.; Damian, R.F.; Rusu, R.D. Biocompatibility of Polyimides: A Mini-Review. *Materials* **2019**, *12*, 3166. [CrossRef]
22. Lee, J.; Kwon, H.; Seo, J.; Shin, S.; Koo, J.H.; Pang, C.; Son, S.; Kim, J.H.; Jang, Y.H.; Kim, D.E.; et al. Conductive fiber-based ultrasensitive textile pressure sensor for wearable electronics. *Adv. Mater.* **2015**, *27*, 2433–2439. [CrossRef]
23. Wu, R.; Ma, L.; Hou, C.; Meng, Z.; Guo, W.; Yu, W.; Yu, R.; Hu, F.; Liu, X.Y. Silk Composite Electronic Textile Sensor for High Space Precision 2D Combo Temperature–Pressure Sensing. *Small* **2019**, *15*, e1901558. [CrossRef]
24. Ma, L.; Liu, Q.; Wu, R.; Meng, Z.; Patil, A.; Yu, R.; Yang, Y.; Zhu, S.; Fan, X.; Hou, C.; et al. From Molecular Reconstruction of Mesoscopic Functional Conductive Silk Fibrous Materials to Remote Respiration Monitoring. *Small* **2020**, *16*, e2000203. [CrossRef] [PubMed]
25. Pouyan, M.B.; Birjandtalab, J.; Heydarzadeh, M.; Nourani, M.; Ostadabbas, S. A pressure map dataset for posture and subject analytics. In Proceedings of the 2017 IEEE EMBS International Conference on Biomedical & Health Informatics (BHI), Orlando, FL, USA, 16–19 February 2017; pp. 65–68. [CrossRef]
26. Hong, Y.S. Smart Care Beds for Elderly Patients with Impaired Mobility. *Wirel. Commun. Mob. Comput.* **2018**, *2018*, 1780904. [CrossRef]
27. Sakai, K.; Sanada, H.; Matsui, N.; Nakagami, G.; Sugama, J.; Komiyama, C.; Yahagi, N. Continuous monitoring of interface pressure distribution in intensive care patients for pressure ulcer prevention. *J. Adv. Nurs.* **2009**, *65*, 809–817. [CrossRef] [PubMed]
28. Soares, R.S.; Lima, S.B.; Eberhardt, T.D.; Rodrigues, L.R.; Martins, R.S.; Silveira, L.B.; Alves, P.J. Skin temperature as a clinical parameter for nursing care: A descriptive correlational study. *J. Wound Care* **2019**, *28*, 835–841. [CrossRef] [PubMed]
29. Kokate, J.Y.; Leland, K.J.; Held, A.M.; Hansen, G.L.; Kveen, G.L.; Johnson, B.A.; Wilke, M.S.; Sparrow, E.M.; Iaizzo, P.A. Temperature-modulated pressure ulcers: A porcine model. *Arch. Phys. Med. Rehabil.* **1995**, *76*, 666–673. [CrossRef] [PubMed]
30. Linder-Ganz, E.; Gefen, A. The Effects of Pressure and Shear on Capillary Closure in the Microstructure of Skeletal Muscles. *Ann. Biomed. Eng.* **2007**, *35*, 2095–2107. [CrossRef] [PubMed]
31. Lee, C.M.; Jin, S.P.; Doh, E.J.; Lee, D.H.; Chung, J.H. Regional Variation of Human Skin Surface Temperature. *Ann. Dermatol.* **2019**, *31*, 349–352. [CrossRef]
32. Wang, Y.; Zhu, W.; Yu, Y.; Zhu, P.; Song, Q.; Deng, Y. High-Sensitivity Flexible Pressure Sensor with Low Working Voltage Based on Sphenoid Microstructure. *IEEE Sens. J.* **2020**, *20*, 7354–7361. [CrossRef]
33. Chen, Z.; Huang, W.; Zhang, X.; Yuen, M.M.F. A Flexible and Stretchable Resistive Epidermal Pressure Sensor for Health Monitoring. *Proc. Electron. Compon. Technol. Conf.* **2016**, *2016*, 1644–1649. [CrossRef]
34. Geninatti, T.; Bruno, G.; Barile, B.; Hood, R.L.; Farina, M.; Schmulen, J.; Canavese, G.; Grattoni, A. Impedance characterization, degradation, and in vitro biocompatibility for platinum electrodes on BioMEMS. *Biomed. Microdevices* **2015**, *17*, 24. [CrossRef]
35. Plasma Metal Coated Yarns. Available online: https://www.swicofil.com/commerce/basic-information/downloads/plasma-metal-coated-yarn.pdf (accessed on 12 January 2024).

36. Steck, D.; Qu, J.; Kordmahale, S.B.; Tscharnuter, D.; Muliana, A.; Kameoka, J. Mechanical responses of Ecoflex silicone rubber: Compressible and incompressible behaviors. *J. Appl. Polym. Sci.* **2019**, *136*, 47025. [CrossRef]

37. Cheng, M.Y.; Lin, C.L.; Lai, Y.T.; Yang, Y.J. A polymer-based capacitive sensing array for normal and shear force measurement. *Sensors* **2010**, *10*, 10211–10225. [CrossRef] [PubMed]

38. Lee, H.K.; Chung, J.; Chang, S., II; Yoon, E. Real-time measurement of the three-axis contact force distribution using a flexible capacitive polymer tactile sensor. *J. Micromechanics Microengineering* **2011**, *21*, 035010. [CrossRef]

39. Dobrzynska, J.A.; Gijs, M.A.M. Flexible polyimide-based force sensor. *Sens. Actuators A Phys.* **2012**, *173*, 127–135. [CrossRef]

40. Wang, Y.C.; Chen, T.Y.; Chen, R.; Lo, C.Y. Mutual capacitive flexible tactile sensor for 3-D image control. *J. Microelectromechanical Syst.* **2013**, *22*, 804–814. [CrossRef]

41. Liang, G.; Wang, Y.; Mei, D.; Xi, K.; Chen, Z. Flexible Capacitive Tactile Sensor Array with Truncated Pyramids as Dielectric Layer for Three-Axis Force Measurement. *J. Microelectromechanical Syst.* **2015**, *24*, 1510–1519. [CrossRef]

42. Chandra, M.; Ke, S.Y.; Chen, R.; Lo, C.Y. Vertically stacked capacitive tactile sensor with more than quadrupled spatial resolution enhancement from planar arrangement. *Sens. Actuators A Phys.* **2017**, *263*, 386–390. [CrossRef]

43. Münzenrieder, N.; Vogt, C.; Petti, L.; Salvatore, G.; Cantarella, G.; Büthe, L.; Tröster, G. Oxide Thin-Film Transistors on Fibers for Smart Textiles. *Technologies* **2017**, *5*, 31. [CrossRef]

44. Zysset, C.; Münzenrieder, N.; Kinkeldei, T.; Cherenack, K.; Tröster, G. Woven active-matrix display. *IEEE Trans. Electron Devices* **2012**, *59*, 721–728. [CrossRef]

45. Rêgo, A.S.; Filipe, L.; Dias, R.A.; Alves, F.S.; Queiroz, J.; Ainla, A.; Arruda, L.M.; Fangueiro, R.; Bouçanova, M.; Bernardes, R.A.; et al. End-User Assessment of an Innovative Clothing-Based Sensor Developed for Pressure Injury Prevention: A Mixed-Method Study. *Int. J. Environ. Res. Public Health* **2023**, *20*, 4039. [CrossRef]

46. Jung, T.M.; Jang, D.J.; Lee, J.H. The Novel Digital Therapeutics Sensor and Algorithm for Pressure Ulcer Care Based on Tissue Impedance. *Sensors* **2023**, *23*, 3620. [CrossRef] [PubMed]

47. Agueda, J.R.S.; Lim, J.; Mondragon, J.M.; Madrid, J.; Belen, M.G.; Eustaquio, G.M.Y.; Monjardin, J.G.; Salud, N. Rapid prototyping of a temperature, humidity, and pressure monitor electronic layer for Pressure Ulcer wound patch. *J. Phys. Conf. Ser.* **2021**, *2071*, 012024. [CrossRef]

48. Lin, Y.H.; Chen, Y.C.; Cheng, K.S.; Yu, P.J.; Wang, J.L.; Ko, N.Y. Higher periwound temperature associated with wound healing of pressure ulcers detected by infrared thermography. *J. Clin. Med.* **2021**, *10*, 2883. [CrossRef] [PubMed]

49. Pickham, D.; Berte, N.; Pihulic, M.; Valdez, A.; Mayer, B.; Desai, M. Effect of a wearable patient sensor on care delivery for preventing pressure injuries in acutely ill adults: A pragmatic randomized clinical trial (LS-HAPI study). *Int. J. Nurs. Stud.* **2018**, *80*, 12–19. [CrossRef]